

Compact camera for multispectral and conventional imaging based on patterned filters

Torbjørn Skauli,* Hans Erling Torkildsen, Stephane Nicolas, Thomas Opsahl, Trym Haavardsholm, Ingebjørg Kåsen, and Atle Rognmo

Norwegian Defence Research Establishment (FFI), P.O. Box 25, 2027 Kjeller, Norway

*Corresponding author: torbjorn.skauli@ffi.no

Received 7 January 2014; revised 25 March 2014; accepted 26 March 2014;
posted 26 March 2014 (Doc. ID 202700); published 21 April 2014

A multispectral camera concept is presented. The concept is based on using a patterned filter in the focal plane, combined with scanning of the field of view. The filter layout has stripes of different bandpass filters extending orthogonally to the scan direction. The pattern of filter stripes is such that all bands are sampled multiple times, while minimizing the total duration of the sampling of a given scene point. As a consequence, the filter needs only a small part of the area of an image sensor. The remaining area can be used for conventional 2D imaging. A demonstrator camera has been built with six bands in the visible and near infrared, as well as a panchromatic 2D imaging capability. Image recording and reconstruction is demonstrated, but the quality of image reconstruction is expected to be a main challenge for systems based on this concept. An important advantage is that the camera can potentially be made very compact, and also low cost. It is shown that under assumptions that are not unreasonable, the proposed camera concept can be much smaller than a conventional imaging spectrometer. In principle, it can be smaller in volume by a factor on the order of several hundred while collecting the same amount of light per multispectral band. This makes the proposed camera concept very interesting for small airborne platforms and other applications requiring compact spectral imagers. © 2014 Optical Society of America

OCIS codes: (040.1490) Cameras; (100.4145) Motion, hyperspectral image processing; (110.4234) Multispectral and hyperspectral imaging; (120.0280) Remote sensing and sensors.

<http://dx.doi.org/10.1364/AO.53.000C64>

1. Introduction

Multispectral and hyperspectral imaging techniques can exploit spectral information to generate information products not available with conventional imaging. Examples include vegetation index mapping, land cover mapping, environmental monitoring, and target detection. Spectral imagers tend to be relatively large because of the optics used to extract spectral information. An imaging spectrometer, for example, employs three sets of imaging optics, a slit and a grating or prism. However, there are important practical cases where a compact camera is

needed, such as for lightweight unmanned aerial vehicles (UAVs) or handheld equipment, and new camera concepts are being developed for such needs [1–3]. Here we discuss a camera concept for applications where moderate spectral resolution is sufficient, or where spectral resolution must be traded for maximum compactness.

The most compact types of spectral imager employ a patterned spectral filter on the image sensor of a regular camera. Most commonly used is the three-band Bayer filter for color photography. In that case, images with good visual quality are obtained by “demosaic” processing of a single image frame. For applications based on quantitative analysis of spectral information, it is often desirable to have more than three bands. However, extending the filter

1559-128X/14/130C64-08\$15.00/0

© 2014 Optical Society of America

array to larger band count increases the lateral separation between filters for different bands and leads to progressively higher misregistration between bands in a single image frame. A possible solution is to place a patterned filter in the entrance aperture, and use an array of microlenses to map the filter onto individual detector elements [4]. This approach enables snapshot imaging with higher band counts at the expense of spatial resolution. Alternatively, a patterned filter in the focal plane can be combined with scanning so that each point in the scene is imaged in all bands. This concept is commonly used in remote sensing satellites employing linear array detectors with different spectral filters. Yet another concept employs a “linear variable filter” (LVF) in front of a 2D array image sensor [5], enabling recording of a large number of spectral bands when the field of view is scanned over the scene.

For multispectral imaging concepts based on patterned filters in the focal plane, the scan motion must be accurately known to ensure spatial coregistration of the different spectral bands. Otherwise there is risk of significant errors in the recorded spectral information, which can significantly degrade the data quality [6,7]. Furthermore, it is potentially problematic that the different spectral bands are recorded at different viewing angles and different times, since the accuracy of the recorded spectrum depends on the angular and temporal variations of the scene spectra, as we discuss below.

Line scan or LVF imagers have normally been built as separate instruments. In some applications, such as UAVs, a spectral imager is often used together with a conventional 2D imaging camera [8]. An interesting exception is [9], where a hyperspectral LVF image sensor is combined with a separate color image sensor behind a common objective lens to form a compact camera for both hyperspectral and conventional imaging.

Along similar lines, we present a camera concept [10] for applications where scanning can be used, for example on a UAV where the platform motion provides the scanning. A multiband filter in the focal plane is patterned so that each band is sampled multiple times during the scan. Only a part of the image sensor area is needed for the multispectral functionality, so that the camera also can be used for conventional 2D imaging. The camera has potential to be used as a compact multifunctional sensor in applications where compactness is essential. We first discuss the camera concept in some detail and then present our implementation in a demonstrator system and the first set of results.

2. Camera Concept

The basic optical layout of the camera is very simple, as shown in Fig. 1(a). An objective lens focuses an image of a scene onto an image sensor with a patterned optical filter. The filter layout has stripes of different bandpass filters across the sensor. By scanning the field of view across the stripes, each scene point

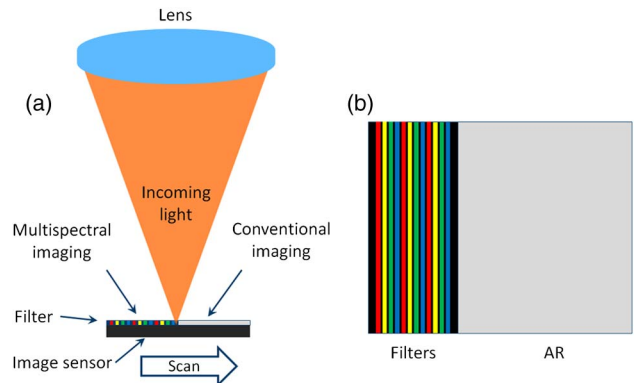


Fig. 1. (a) Sketch of the optical layout of the camera. A patterned filter is placed on the image sensor in the focal plane of an objective lens. (b) Sketch of the filter pattern. The filter has multiple regions with different bandpass characteristics laid out in stripes across the image sensor. Each spectral band is repeated multiple times across the filter. A large part of the image sensor is left unfiltered, for use in conventional imaging.

can be observed through all the different filters, and its spectral properties can be reconstructed.

The image reconstruction is the most difficult aspect of this class of spectral imagers. To record accurate spectral information, it is necessary to track the motion of a scene point accurately in sequential raw images as the point moves across the filter. Data from the raw images must be combined to form a reconstructed output image. Errors in the tracking of scene motion will lead to spatial coregistration errors between bands, potentially resulting in significant errors in the recorded spectra [6,7]. Of course, the images themselves can be used to aid the reconstruction of spectra by tracking scene movements, but the reconstruction remains a nontrivial aspect of this otherwise simple class of spectral imagers. To achieve good spectral coregistration, the output image will typically need to be reconstructed with a lower spatial resolution than the recorded raw images. It is also important to avoid spatial undersampling of the scene in the recording of raw images.

Even if scene movements are tracked correctly, the sequential recording of bands can lead to artifacts in the recorded spectra in two ways: first, if a point in the scene changes in time during the scanning then different bands will tend to represent different states of the scene, leading to errors in the reconstructed spectrum analogous to a spatial coregistration error. Second, if the scan is a linear motion of the camera relative to the scene then different bands view the scene in different angles. If the radiance from the scene depends on viewing angle then spectral artifacts will result. Such angular dependence can easily arise in practice, for example from specular reflections or parallax effects.

Figure 2 illustrates the potentially problematic effect of parallax for the example case of airborne imaging. The different spectral bands are recorded sequentially as the camera moves along the flight

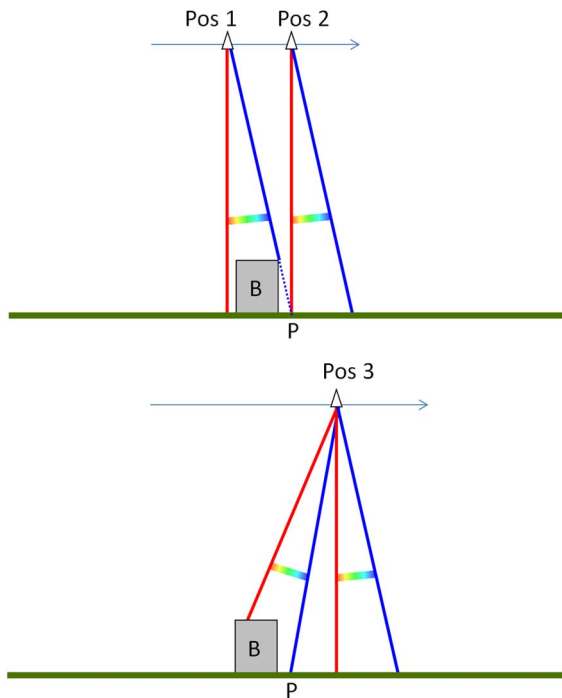


Fig. 2. Parallax effect on the recorded spectrum. Top: a camera that makes a single sample in each band. The arrow indicates the motion of the camera in an airborne imaging application. Red and blue lines indicate lines of sight for the leading and trailing band for two positions along the scan motion, with other bands in between as suggested by the “spectrum” bar. The green line indicates ground with a point P to be observed, and a building B causes parallax effects, see text. Bottom: a camera that samples each band twice can overcome the parallax effect by recording missing data for point P at a later position in the scan.

path. Typically, the airborne sensor package includes a navigation system, which can be combined with a geometrical model of the terrain to assign a scene position for each recorded pixel. By such georeferencing, it is possible to estimate the amount of light in each spectral band coming from each point in the scene under the flight path, and to construct a spectral image of the terrain. However, the spectrum estimation must make the assumption that the radiance received from the scene is independent of viewing angle during the recording. As seen in Fig. 2, the assumption will not always be valid. In this example case, the trailing “red” band records light from point P on the ground when the camera is at position 2. However, in position 1, the leading “blue” band sees the roof of the building B, which obscures point P. Thus, because of parallax effects, a valid spectrum cannot be obtained for point P. At best, given detailed knowledge of scene geometry, this point can be labeled as invalid in the reconstructed image. These concerns are the same for a camera based on LVF.

To minimize signal errors due to time- and angle-dependent scene radiance, the extent of the filter should be minimized in the scan direction. In addition, we introduce multiple repetitions of the filter pattern along the scan direction, as indicated in Fig. 1(b). In the example in Fig. 2, the blue band

can be sampled for point P at a later point in the scan if the camera records the bands multiple times. The repeated sampling enables several different strategies for minimizing spectral error, depending on what assumptions can be made about the scene. For smooth angular variations, averaging multiple readings of each band interspersed with the other bands will tend to produce a spectrum representing the scene properties at the middle of the scan. For abrupt variations, such as the parallax case in Fig. 2, a voting scheme can be implemented, or consistency checks can be used to flag unreliable data.

Even with repeated sampling, the extent of the filter may easily be made much shorter in the scan direction than across the scan. This is illustrated by the experimental realization below. For image sensors with normal formats, a large fraction of the sensor area (as well as of the image circle of the optics) might then be left unused. This area can conveniently be used for conventional imaging, as indicated in Fig. 1(b). The resulting camera is then capable of recording multispectral still images by scanning, but it can also be used to record conventional 2D video or still images, all in a very compact package. It can be noted that the image sensor must be capable of handling the larger signal dynamics resulting from having filtered and unfiltered regions, but this is feasible using state-of-the-art silicon image sensors.

Clearly, the 2D images can be used to support the reconstruction of spectral images in various ways, such as by estimation of optical flow. An interesting aspect is that the 2D imagery can be used for reconstructing the 3D structure of the scene. This is useful in itself, and a 3D scene model can also be very helpful for the spectral reconstruction, as pointed out in [9].

3. Experimental Realization

For our demonstrator, we have selected six bands in the visible and near-infrared (VNIR) spectral range where silicon-based image sensors are readily available. This number of bands is a compromise between fabrication cost and predicted performance. To select the spectral bands, we have used a set of hyperspectral images of natural scenes to synthesize image data for various choices of bands. We have then tested the discriminability of various objects in the images for different band combinations [11]. Somewhat unsurprisingly, we find that good performance is obtained for spectral bands similar to those used on earth observation satellites. It is potentially useful to relate the recorded images to the literature on satellite remote sensing, therefore we choose the bands shown in Fig. 3. This set of bands also enables rendering of RGB color images, using bands 1, 2, and 4.

The patterned multiband interference filter is deposited on a glass substrate. The layout is indicated in Fig. 4. Measured transmission spectra for all six bands are shown in Fig. 5. The filters are laid out

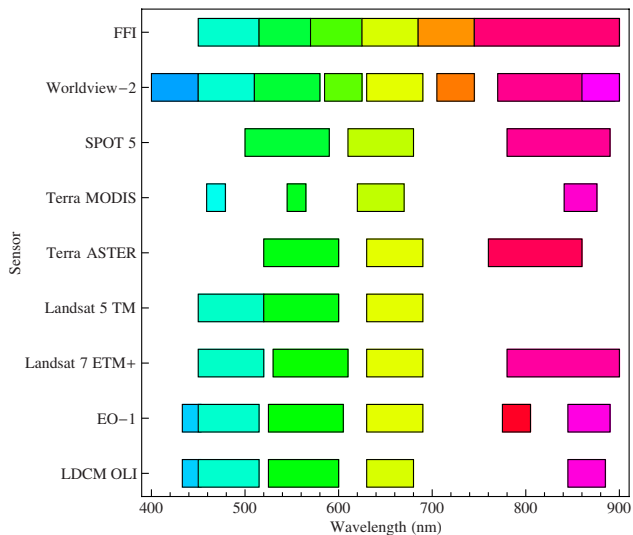


Fig. 3. Chosen spectral bands (top) in comparison with VNIR bands of various earth observation satellites.

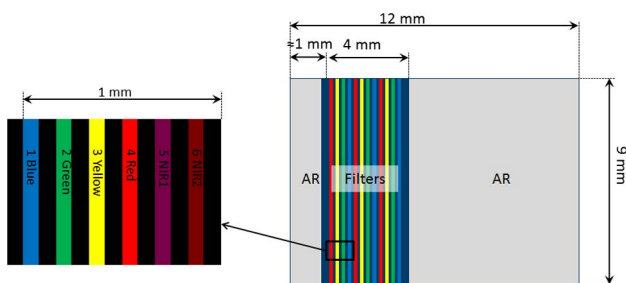


Fig. 4. Layout of the filter for the demonstrator system. Stripes of six different bandpass filters extend across the image sensor, orthogonal to the nominal scan direction. The set of filters is repeated four times. The neighboring areas of the filter substrate are AR coated.

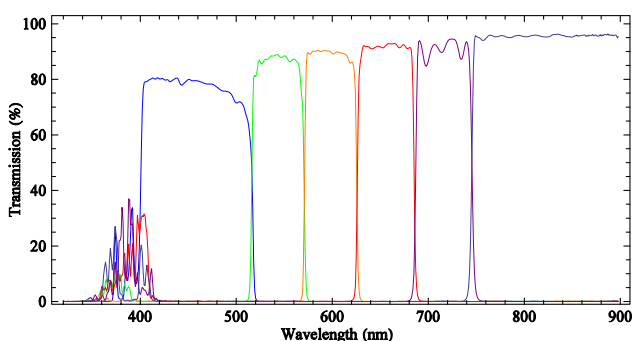


Fig. 5. Measured transmission spectra of the bandpass filters at normal incidence.

in 86 μm wide stripes across the image sensor, separated by 80 μm wide shadow masks to avoid cross talk between bands. For the 7.4 μm pixel pitch, the filter stripes correspond to about 10 unobscured detector pixels across each stripe. The six bands take up a total width of 1 mm, and are repeated four times

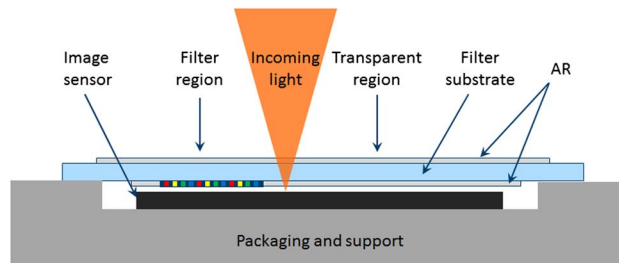


Fig. 6. Sketch of the focal plane assembly. The filter is placed close to the image sensor. The filter substrate extends across the entire sensor, with only AR coating on the unfiltered parts.

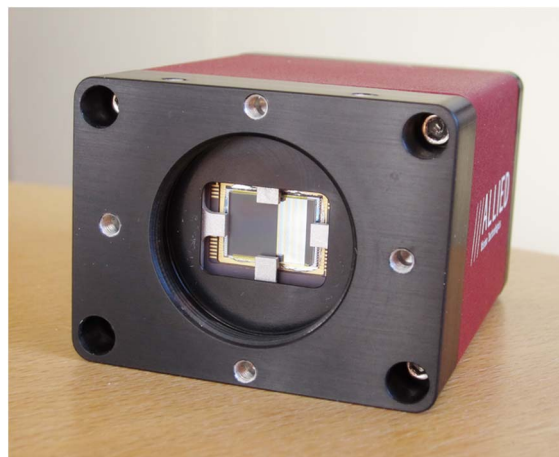


Fig. 7. Front view of the assembled camera without lens. The patterned filter covers the right part of the image sensor. A metal fixture holds the filter substrate in place.

for a total filter width of 4 mm in the scan direction. The remaining areas of the filter substrate are anti-reflection (AR) coated. This leaves more than half of the image sensor area for conventional panchromatic 2D imaging. A narrow unfiltered region is left on the outer side of the filter stripes, near the edge of the image sensor, intended for use in motion tracking across the filter region.

Here we use an AVT GE1650 camera based on a Truesense KAI-2020 monochrome CCD with 1600×1200 pixels and 7.4 μm pixel pitch. The filter is placed very close (approximately 20 μm) to the image sensor, essentially forming a proximity focus of the filter pattern, as indicated in Fig. 6. (It is possible to deposit patterned filters during the production of an image sensor, with potential for low-cost manufacturing of large production series. However, this requires significant effort in process development and is thus not a viable option for a demonstrator system.) The outer band limits are set by a filter in front of the objective lens, which blocks radiation outside the range 450–900 nm. Figure 7 shows the assembled camera without the lens. The filter is held in place by a mechanical clamp, with spacers between the filter and the CCD to create an air gap of about 20 μm . For the demonstrator system we use

objective lenses which are optically corrected and AR-coated for the VNIR spectral range.

4. Angle Dependence of Filter Characteristics

In this camera concept, appropriate design flexibility and performance can only be achieved by employing interference filters, whose spectral properties depend on the angle of incidence. This becomes a concern here, since angular variations at the filter are inherent to the concept: the focused cone of light from a scene point spans a range of angles of incidence according to the numerical aperture of the lens, inevitably leading to some broadening of the spectral features of the filter. In addition, the angle of the principal ray of the cone varies according to the viewing direction for a conventional lens. However, if the lens is image-side telecentric then this latter angular variation can be avoided.

Spectral features of an interference filter tend to shift to shorter wavelengths with increasing angle of incidence. The relative wavelength shift $\Delta\lambda$ at an angle of incidence θ can be approximated by [12]

$$\frac{\Delta\lambda}{\lambda} \approx \sqrt{1 - \left(\frac{\sin \theta}{n_e}\right)^2} - 1 \approx -\frac{\theta^2}{2n_e^2}, \quad (1)$$

where n_e is an effective refractive index for the filter stack.

Figure 8 shows measured spectra for the green band at incidence angles of 0, 12, and 25 deg. There is a significant spectral shift for this relatively large change in angle of incidence. From similar measurements of all spectral edges in the six-band filter, we find that the wavelength shifts can be approximated by Eq. (1) assuming an effective refractive index $n_e \approx 1.7$. The approximated amount of spectral shift is plotted in Fig. 9. Due to the square dependence on angle, the shift can be significant in some cases and insignificant in others, as we discuss in the following.

The influence of incidence angle on the recorded spectral signal can be estimated by assuming a step-shaped spectrum where two neighboring bands have spectral radiances L_1 and L_2 , constant within each band. Nominally, these are the values recorded

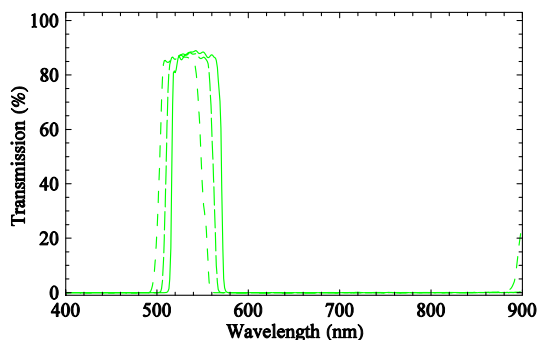


Fig. 8. Measured transmission spectrum of the filter for the green band at 0 deg (solid), 12 deg (long dash), and 25 deg (short dash) angle of incidence.

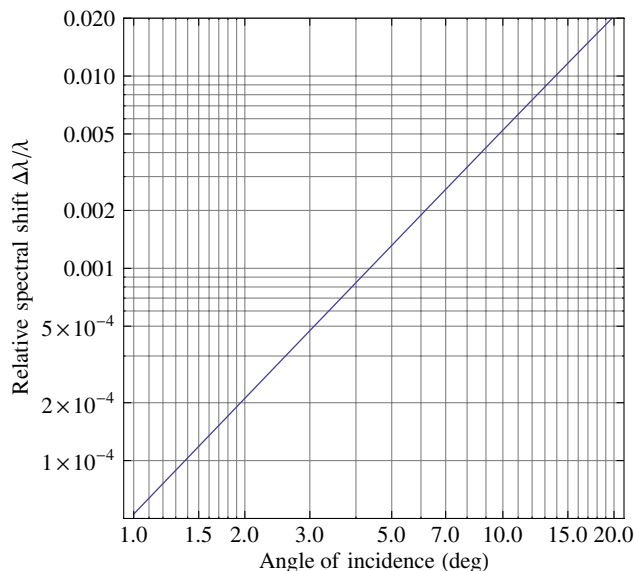


Fig. 9. Relative shift of spectral features of the filter for varying angle of incidence, according to the approximation (Eq. 1), assuming an effective refractive index $n_e = 1.7$.

by the camera. Let λ_1 and λ_2 be the nominal boundaries of band 1. Now assume that the band is shifted by $\Delta\lambda$ toward band 2. The radiometric distortion of the signal S_1 in band 1 becomes

$$\Delta S_1 = \frac{\Delta\lambda}{\lambda_2 - \lambda_1} \frac{L_1 - L_2}{L_1} S_1. \quad (2)$$

Assuming that the spectral contrast is such that $L_2 < L_1$, then in the worst case $(L_1 - L_2)/L_1$ is approximately unity and the maximum signal distortion is determined by the ratio of spectral shift to band width. If band 1 is taken to have the largest spectral radiance of all bands, then Eq. (2) represents the maximum possible error in recorded radiance over all bands for a step-shaped spectrum. This may be a reasonable estimate of errors in many practical cases, noting for example that reflectance spectra of solids in the VNIR range tend to be smooth. In other cases, such as for a line-shaped spectrum, Eq. (2) will underestimate the error due to spectral shift.

The effect of angle tuning across the field of view should ideally be less than the noise. For our camera, a single pixel in a raw image will have an RMS noise of the order of 1%, assuming a partial well fill of 10,000 electrons with Poisson noise as the dominating noise source. However, a pixel in the final output image will typically be an average of multiple raw pixels since the filter layout provides for sampling a scene point about 40 times and since the raw image pixels normally will be resampled to somewhat larger output pixels. Therefore, it can be argued that the output noise level may become significantly lower than 1% from averaging over multiple input pixels, depending on the details of the application.

The chosen bands here have a total width of the order of 10% of the wavelength. If a signal error of up to 1% is permitted then, according to Eq. (2), the spectral shift must be less than about 1% of the bandwidth, or 0.1% of the wavelength. The largest permissible angle of incidence is then about 4 deg according to Fig. 9. If a lower noise level is taken as reference then the variation in angle of incidence will need to be even less. This shows that it is strongly preferable to use an objective lens that is image-side telecentric, so that the focus cone spans the same range of incidence angles on the filter independently of the position in the field of view. The spectral broadening due to angular variation within the focus cone will be relatively unproblematic for telecentric lenses with moderate numerical aperture. If, for example, a broadening of about 10% of the bandwidth is allowed then the half-angle of the cone may be as large as 15 deg, corresponding to an F/2 aperture. These estimates of angle tuning effects are based on the properties of the filter used in our demonstrator. Narrower bands will lead to more stringent requirements.

We must point out that the dependence on angle of incidence is a more critical concern in our multispectral camera than in some other filter-based spectral camera concepts where the angular variations can be calibrated out. For an LVF-based camera, for example, angular variation across the field of view can be compensated by mapping the resulting shift in filter wavelength across the image sensor and postprocessing the image data accordingly. This is not possible with our set of discrete bandpass filters. On the other hand, the concept presented here enables repeated sampling of bands, which also helps to preserve signal integrity.

5. Light Collection and Camera Size

Photon noise can lead to significant degradation of spectral image processing results [13], especially in low-light scenes. This is a challenge for commonly used hyperspectral imagers, such as imaging spectrometers and LVF-based cameras, where a very large fraction of the incoming light is rejected, in the slit or filter, respectively. Noise properties of hyperspectral and multispectral imagers can only be compared in cases where the image analysis is not significantly helped by the higher spectral resolution of a hyperspectral camera. This can be the case if photon noise is dominating, or if the bands chosen for the multispectral imager are well adapted to the task at hand. For such a case, we now compare the light collection capability of our camera to that of an imaging spectrometer.

Assume that input pupil area, pixel size, and scan speed are identical so that multispectral and hyperspectral imaging runs at the same integration time. Assume that images from the spectrometer are formed by averaging groups of bands in the hyperspectral image to match the bands of the multispectral camera. For a given pixel, the imaging

spectrometer collects light in one integration time, while the multispectral camera would see the same pixel over 10 integration times in each of four filter stripes (each 10 pixels wide) for a given band. This gives 40 times more light, although admittedly the comparison makes assumptions that are favorable to the multispectral camera. The input pupil area of the multispectral camera could then be reduced by a factor 40 and collect the same amount of light as the imaging spectrometer, in principle. The volume of a camera scales roughly with the input pupil diameter cubed. Recall also that an imaging spectrometer has three sets of imaging optics (in front of slit, disperser, and image sensor). Thus, under our assumptions the multispectral camera could be made a factor $3 \times 40^{3/2} = 760$ smaller in volume. Even if assumptions here were optimistic, this very large factor indicates that the multispectral camera is an interesting alternative to hyperspectral imaging wherever compactness is essential.

6. Preliminary Imaging Results

As a first test, we have used a rotary stage to scan the camera across a simple scene in the lab using an 85 mm focal length lens (Zeiss Planar 1.4/85 ZF-IR) set at F/4. The resulting field of view is small, and we neglect angle tuning and geometrical distortions. The camera was radiometrically calibrated using a reference lamp. The scan movement was nominally 1 pixel horizontally between successive images, but with some irregularity due to inadvertent software jitter. The resulting data then serve to illustrate some challenges that could be encountered in a practical application, for example, a turreted camera on a ground vehicle. We have implemented a relatively simple processing chain for initial image reconstruction. Sample results are shown in Fig. 10.

First, a panchromatic mosaic of the scene is created from the unfiltered part of a small subset of the images. This provides a common reference for all images in the sequence. Individual images are then related to the reference image by a homography estimated from a set of corresponding point pairs in the reference image and the unfiltered image section in each image, illustrated in Fig. 10(a). Since the camera undergoes a rotational scanning motion, the homography is simply estimated from RANSAC inliers using the direct linear transformation [14]. The estimated homography for a given frame can then be used to position the spectrally filtered pixels in the pixel coordinate system defined by the panchromatic reference image. For this initial image reconstruction we use a single column of pixels from each stripe in the filter and assign them to the nearest neighbor in the reference image. This results in 24 images representing the 24 filter stripes. The final image is obtained by averaging groups of four images corresponding to the same spectral band.

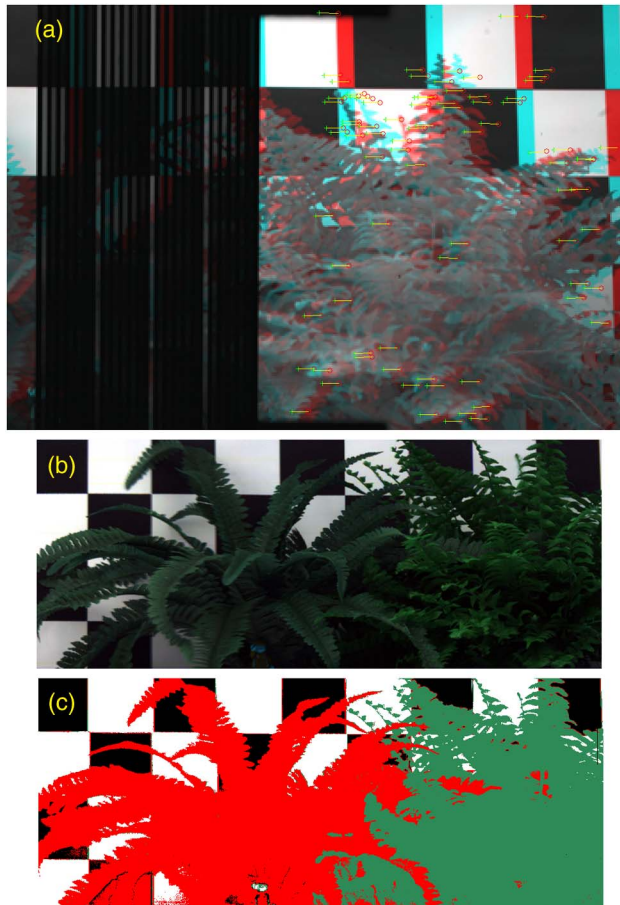


Fig. 10. Example images recorded in the lab. The scene consists of a real and an artificial plant with a checkerboard background. (a) Two superimposed raw images showing the point correspondences used to estimate the transformation between them. The stripe pattern of filters and shadow masks is seen on the left. (Shaded areas at the top and bottom are due to the clamp holding the filter.) (b) Reconstructed RGB image after averaging multiple spectral samples in each pixel. (c) Result of maximum likelihood spectral classification.

An RGB representation of the final image is shown in Fig. 10(b).

The nearest neighbor pixel assignment leads to a few gaps in the 24 intermediate images due to scan irregularities, but these gaps are eliminated in the averaging step. This illustrates one benefit of the multiple sampling of each band. Otherwise this preliminary reconstruction is obviously suboptimal in many ways, such as by not using all raw pixels and by employing a simplistic nearest-neighbor resampling strategy.

Finally, the image in Fig. 10(c) shows the result of a maximum likelihood spectral classification using a set of multinormal distributions to represent the main materials in the image. Distribution parameters have been estimated from a small sample of each material in the same image. The classification mostly works well, but with notable misclassifications at the black–white transitions in the background. This strongly suggests imperfect coregistration of the

spectral bands, which is unsurprising given the simplistic reconstruction used here.

7. Discussion and Conclusions

We have presented a concept for multispectral imaging based on patterned filters in the focal plane and scanning of the field of view. As with many other spectral imaging techniques, there is a risk of spectral artifacts if the radiance from the scene varies with angle or time within the scan. Here, we minimize the risk of spectral errors by making the filter short in the scan direction and by repeated interspersed sampling of the spectral bands. The repeated sampling enables strategies to preserve the integrity of the spectral signal, such as the averaging and gap-filling in our preliminary image reconstruction. Still, the image reconstruction remains a main challenge for this class of spectral imagers. On the other hand, there is potential to make the camera very compact. Spatial downsampling may be necessary to obtain an output image with good coregistration of bands. Angular dependence of the filter characteristics is a potential issue which can be managed by appropriate choice of objective lens.

By minimizing the extent of the filter in the scan direction, most of the image sensor area can be used for conventional 2D still or video imaging. The 2D imagery can be used to support the reconstruction of spectral images, as demonstrated by a simple example here. In cases where the scan is a linear motion, it will also be helpful to use the 2D imagery to reconstruct the 3D shape of the scene.

In summary, the multispectral imaging concept presented here offers a multifunctional camera in a compact package. The concept also has disadvantages, notably the limited spectral resolution and the nonsimultaneous sampling of bands. Still the concept appears attractive in applications where compactness and light weight is critical, since it has potential to bring down the size of spectral imaging sensors from kilos to grams.

References

1. N. Tack, A. Lambrechts, P. Soussan, and L. Haspeslagh, "A compact high-speed and low-cost hyperspectral imager," *Proc. SPIE* **8266**, 82660Q (2012).
2. H. Saari, V.-V. Aallos, C. Holmlund, J. Mäkynen, B. Delauré, K. Nackaerts, and B. Michiels, "Novel hyperspectral imager for lightweight UAVs," *Proc. SPIE* **7668**, 766805 (2010).
3. M. Pisani and M. Zucco, "Compact imaging spectrometer combining Fourier transform spectroscopy with a Fabry–Perot interferometer," *Opt. Express* **17**, 8319–8331 (2009).
4. D. B. Cavanaugh, J. M. Lorenz, N. Unwin, M. Dombrowski, and P. Wilson, "VNIR hypersensor camera system," *Proc. SPIE* **7457**, 745700 (2009).
5. A. M. Mika, "Linear-wedge spectrometer," *Proc. SPIE* **1298**, 127–131 (1990).
6. P. Mouroulis, R. O. Green, and T. G. Chrien, "Design of pushbroom imaging spectrometers for optimum recovery of spectroscopic and spatial information," *Appl. Opt.* **39**, 2210–2220 (2000).
7. T. Skauli, "An upper-bound metric for characterizing spectral and spatial coregistration errors in spectral imaging," *Opt. Express* **20**, 918–933 (2012).

8. X. Sun, "Computerized component variable interference filter imaging spectrometer system method and apparatus," U.S. patent 6,211,906 (3 April 2001).
9. J. Biesemans, B. Delaure, and B. Michiels, "Geometric referencing of multi-spectral data," Patent application EP2513599 A1 (2012).
10. T. Skauli, "Imaging unit," Patent application NO20130382 (2013).
11. I. Kåsen, A. Rødningsby, T. V. Haavardsholm, and T. Skauli, "Band selection for hyperspectral target-detection based on a multinormal mixture anomaly detection algorithm," Proc. SPIE **6966**, 696606 (2008).
12. W. J. Smith, *Modern Optical Engineering*, 3rd ed. (McGraw-Hill, 2000), p. 208.
13. T. Skauli, R. Ingebrigtsen, and I. Kåsen, "Effect of light level and photon noise on hyperspectral target detection performance," Proc. SPIE **6661**, 66610D (2007).
14. R. Harley and A. Zisserman, *Multiple View Geometry in Computer Vision*, 2nd ed. (Cambridge University, 2003).